

# Orbital hybridization and covalency in paraelectric and ferroelectric $\text{SrBi}_2\text{Nb}_2\text{O}_9$

Y. Shimakawa, H. Imai, H. Kimura, S. Kimura, and Y. Kubo

*Fundamental Research Laboratories, NEC Corporation, 34 Miyukigaoka, Tsukuba 305-8501, Japan*

E. Nishibori, M. Takata, and M. Sakata

*Department of Applied Physics, Nagoya University, Furo-cho, Nagoya 464-8601, Japan*

K. Kato

*Japan Synchrotron Radiation Research Institute, 1-1-1 Kouto, Mikazuki-cho, Hyogo 679-5198, Japan*

Z. Hiroi

*Institute for Solid State Physics, University of Tokyo, 5-1-1 Kashiwanoha, Kashiwa 277-8581, Japan*

(Received 19 June 2002; revised manuscript received 22 August 2002; published 31 October 2002)

Electron-density distributions of paraelectric and ferroelectric  $\text{SrBi}_2\text{Nb}_2\text{O}_9$  were analyzed by means of synchrotron x-ray diffraction. The obtained electron-density distributions well reproduced the atomic arrangements of the material. Bonding electrons due to hybridization of orbitals were clearly seen in the Nb-O bonds in the octahedron and in the Bi-O bonds in the  $\text{Bi}_2\text{O}_2$  layer. The hybridization between Nb(4*d*) and O(2*p*) orbitals was enhanced in the ferroelectric phase, and one of the Nb-O bonds showed a strong covalent character below the ferroelectric Curie temperature. Weak hybridization of the Sr(5*s*) with O(2*p*) orbitals appears to play an important role in structural distortion and ferroelectric polarization. The changes in the electron-density distribution through the ferroelectric phase transition are similar to those observed in ferroelectric  $\text{PbTiO}_3$  perovskite.

DOI: 10.1103/PhysRevB.66.144110

PACS number(s): 77.84.Dy, 61.10.Nz, 77.80.Bh

## I. INTRODUCTION

Ferroelectric thin films have attracted considerable attention for use in nonvolatile memory applications, i.e., ferroelectric random-access memories. Bi-layered compounds are leading candidate materials for such devices and have been extensively studied.<sup>1,2</sup> These materials were discovered in the late 1940's and have often been called Aurivillius compounds,<sup>3-5</sup> and their basic structural and ferroelectric properties were studied in the early 1960's.<sup>6</sup> However, the information obtained at that time was not sufficient to reveal their inherent properties. Recent significant developments in material characterization and electronic-structure calculation techniques promise to provide new insight into these "old" materials.<sup>7-11</sup>

$\text{SrBi}_2\text{Nb}_2\text{O}_9$  (SBN) is one of the Bi-layered compounds and its structure consists of  $\text{Bi}_2\text{O}_2$  layers and perovskite-type  $\text{SrNb}_2\text{O}_7$  units with double  $\text{NbO}_6$  octahedral layers (see Fig. 1). Orthorhombic structural distortion with noncentrosymmetric space group  $A2_1am$  is the origin of the ferroelectric behavior of this material, and the displacement of constituent ions causes spontaneous ferroelectric polarization along the *a* axis.<sup>12,13</sup> We previously used high-resolution neutron diffraction to investigate precise crystal structures of the  $\text{SrBi}_2(\text{Ta}_{1-x}\text{Nb}_x)_2\text{O}_9$  solid-solution system<sup>10</sup> and revealed that some of the (Ta,Nb)-O bonds are shorter than the expected ionic bond length. These short bond lengths suggest that the bonds have a covalent character and that strong covalent interaction appears to play an important role in the ferroelectric properties of the materials.

The importance of covalency in ferroelectric oxides was first pointed out by Cohen and Krakauer in the 1990's

through first-principles electronic-structure calculations of  $\text{PbTiO}_3$  (PTO) and  $\text{BaTiO}_3$  (BTO) perovskites.<sup>14-16</sup> They concluded that the hybridization of orbitals between Ti(3*d*) and O(2*p*) is essential for structural distortion and ferroelectric instability, and Pb(6*s*)-O(2*p*) overlap enhances the ferroelectric polarization. Such orbital hybridization was experimentally confirmed by Kuroiwa *et al.* in terms of electron-density distribution determined from MEM (maximum entropy method) of synchrotron x-ray-diffraction data.<sup>17</sup> Bonding electrons between Ti and O atoms were clearly seen in the obtained electron-density distribution, and the hybridization of the Pb(6*s*) and O(2*p*) orbitals in a ferroelectric PTO sample was evidently enhanced. The results clearly demonstrated that the electron-density distribution determined by MEM gave an important information on the orbital hybridization and covalency in ferroelectric oxides.

In the present study, we analyzed the electron density of paraelectric and ferroelectric  $\text{SrBi}_2\text{Nb}_2\text{O}_9$ . The obtained electron-density distribution below the ferroelectric Curie temperature showed structural distortions. The orbital hybridization and covalency are found to be important factors in ferroelectric properties.

## II. EXPERIMENTS AND RESULTS

A powder sample of  $\text{SrBi}_2\text{Nb}_2\text{O}_9$  was prepared by solid-state reaction. A mixture of appropriate amounts of  $\text{SrCO}_3$ ,  $\text{Bi}_2\text{O}_3$ , and  $\text{Nb}_2\text{O}_5$  was sintered at 1100 °C for 24 h with intermediate grindings and then cooled in the furnace at 2 °C/min. The sample was confirmed to be single phase by x-ray diffraction. The temperature dependence of the dielec-

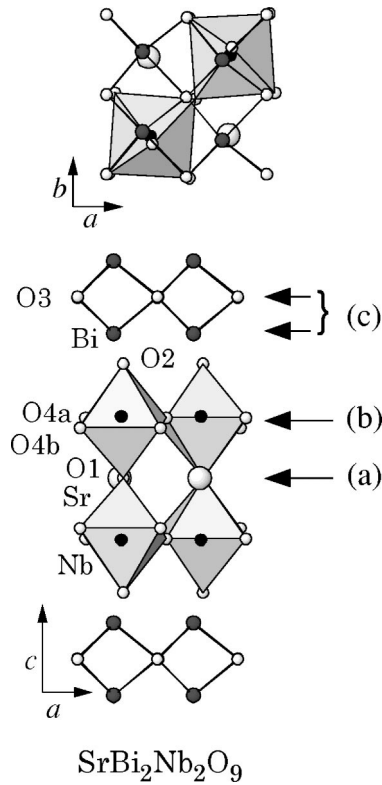


FIG. 1. Crystal structures of  $\text{SrBi}_2\text{Nb}_2\text{O}_9$ . The structure model is drawn with the refined positional parameters of the orthorhombic phase. Upper part of the figure is  $a$ - $b$  projection of the structure, and lower part is  $a$ - $c$  projection of half of the unit cell. See Refs. 7–10 for the nomenclature used in the figure. Arrows (a)–(c) indicate the positions of planes appeared in the contour maps in Fig. 4.

tric constant of the sample was investigated by measuring the capacitance of the disk-shaped samples with a conventional  $LCR$  meter at a frequency of 100 kHz. The determined ferroelectric Curie temperature ( $T_C$ ) was 440 °C (Fig. 2).

The electron-density distribution was determined by MEM of synchrotron x-ray-diffraction data.<sup>18,19</sup> To collect accurate diffraction-intensity data, a fine-powder sample was prepared by precipitation and sealed in a 0.1-mm-diameter quartz capillary. Synchrotron x-ray-diffraction data were collected on a large Debye-Scherrer camera installed on the BL02B2 beam line at SPring-8. The diffraction data for paraelectric and ferroelectric phases were taken at 580 and 25 °C (room temperature), respectively (see Fig. 2). The wavelength of the incident beam was 0.461 Å. Figure 3 shows x-ray-diffraction patterns and the results of preliminary Rietveld refinements for  $\text{SrBi}_2\text{Nb}_2\text{O}_9$  at 580 and 25 °C. The data covering  $2\theta$  from 1.6 to 42.0° were used for the refinements. The observed diffraction pattern of the high-temperature paraelectric phase was well reproduced by the tetragonal structure model with space group  $I4/mmm$ , and the reliability factor from the Rietveld refinement,  $R_1$ , was 3.60%. As shown in the inset of Fig. 3, characteristic orthorhombic reflections, such as  $1\ 2\ 2$  ( $2\theta \approx 9.76^\circ$ ;  $d \approx 2.45$  Å) and  $2\ 1\ 3$  ( $2\theta \approx 10.00^\circ$ ;  $d \approx 2.39$  Å), were extinct in the diffraction pattern taken at 580 °C. This clearly demonstrated that the SBN sample at 580 °C was tetragonal, though

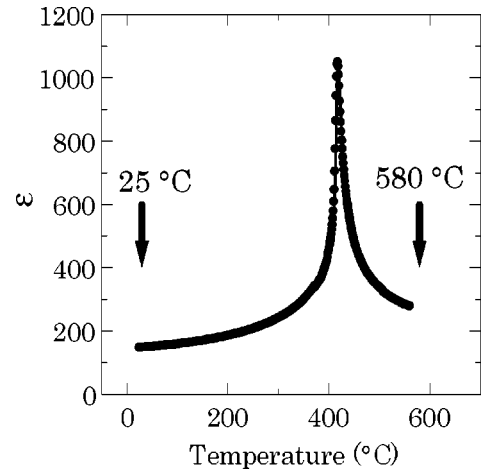


FIG. 2. Temperature dependence of the dielectric constant  $\epsilon$  of  $\text{SrBi}_2\text{Nb}_2\text{O}_9$ . The x-ray diffraction of paraelectric and ferroelectric phases shown in Fig. 3 were taken at 580 and 25 °C, respectively.

recent careful experiments suggested the existence of an intermediate paraelectric and orthorhombic phase immediately above the ferroelectric Curie temperature in the Bi-layered materials.<sup>20,21</sup> Refined positional parameters are listed in Table I. The crystal structure of the room-temperature ferroelectric phase has  $A2_1am$  orthorhombic symmetry and is significantly distorted. Refined structural parameters were essentially the same as previously reported.<sup>10</sup> The reliability factor for the orthorhombic phases was 3.00%.

Each Bragg integrated intensity was determined by a peak-profile fitting by using an auxiliary Rietveld refinement. Note that the MEM provides the most plausible electron-

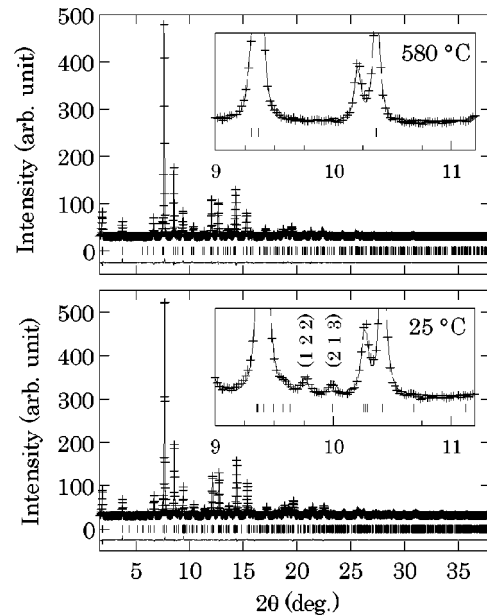


FIG. 3. Synchrotron powder x-ray-diffraction patterns of  $\text{SrBi}_2\text{Nb}_2\text{O}_9$  and Rietveld refinement profiles. The observed diffraction data are shown as plus marks, and the calculated profile as a solid line. Tick marks below the profile indicate the positions of allowed reflections. Differences between the observed and calculated intensities are shown at the bottom.

TABLE I. Refined structural parameters of high-temperature tetragonal  $\text{SrBi}_2\text{Nb}_2\text{O}_9$ . Numbers in parentheses are standard deviations of the last significant digit. All the occupation factors were fixed at 1. Space group;  $I4/mmm$ .  $a=3.96570(3)$  Å and  $c=25.4879(5)$  Å. Note that  $R_{\text{wp}}=1.01\%$ ,  $R_1=3.60\%$ , and  $R_F=3.54\%$ .

Atom	Position	$x$	$y$	$z$
Sr	$2a$	0	0	0
Bi	$4e$	0	0	0.201 21(5)
Nb	$4e$	0	0	0.413 87(6)
O1	$2b$	0	0	0.5
O2	$4e$	0	0	0.344 9(6)
O3	$4d$	0	0.5	0.25
O4	$8g$	0	0	0.423 2(3)

density distribution from structure factors, i.e., the diffraction intensities, without the need for any internal structural parameters. The integrated intensities of 198 and 558 independent Bragg peaks of the tetragonal and orthorhombic phases, respectively, were obtained from the diffraction data for  $d$  spacing down to 0.75 Å. The electron-density distributions were analyzed by using the program MEED.<sup>22</sup> The unit cells of paraelectric tetragonal ( $3.97 \times 3.97 \times 25.49$  Å<sup>3</sup>) and ferroelectric orthorhombic ( $5.58 \times 5.57 \times 25.36$  Å<sup>3</sup>) phases were divided into  $28 \times 28 \times 164$  and  $36 \times 36 \times 164$  pixels, respectively. The volume of one pixel corresponds to about  $0.15 \times 0.15 \times 0.15$  Å<sup>3</sup>. The  $R$  factors of the MEM were lower than those of the Rietveld refinements and became 2.94% and 2.71% for the tetragonal and orthorhombic phases, respectively. Although cation disorder between Sr and Bi in  $\text{SrBi}_2(\text{Nb,Ta})_2\text{O}_9$  was recently reported,<sup>13,23</sup> we confirmed

that the final electron-density distributions were little affected by whether the preliminary structure models had such cation disorder or not. Figure 4 shows the contour map of electron-density distributions of SrO, NbO<sub>2</sub>, and Bi<sub>2</sub>O<sub>2</sub> planes perpendicular to the  $c$  axis (see Fig. 1 for the positions of the planes). The electron densities along the  $c$  axis are also shown in the figure. The obtained electron-density distributions well reproduced the atomic arrangements of  $\text{SrBi}_2\text{Nb}_2\text{O}_9$ , and some bonding electrons are clearly seen in the distributions.

The hybridization of orbitals was examined by electronic-structure calculations. The program CRYSTAL was used for *ab initio* calculation based on the density functional theory using local density approximation.<sup>24</sup> Since the orthorhombic structure is rather complicated and the number of orbitals concerned is too large to calculate, only the electronic structure of the tetragonal phase is considered. Refined positional parameters obtained from the preliminary Rietveld refinement listed in Table I were used for the calculation. We used optimized basis sets with effective core potentials (ECP):<sup>25</sup>  $2(sp)$ ,  $2(p)$ , and  $1(d)$  shells with  $[\text{Xe}](4f)^{10}(5d)^{10}$  ECP for Bi,  $2(sp)$ ,  $2(p)$ , and  $1(d)$  shells with  $[\text{Ar}](3d)^{10}$  ECP for Sr,  $3(sp)$ ,  $3(p)$ , and  $2(d)$  shells with  $[\text{Ar}](3d)^{10}$  ECP for Nb, and  $2(sp)$  and  $2(p)$  shells with  $[\text{He}]$  ECP for O. The calculated total density of states (DOS), the partial DOS for Nb and O atoms in the perovskite-type unit, and the partial DOS for Bi and O atoms in the Bi<sub>2</sub>O<sub>2</sub> layer are shown in Fig. 5.

### III. DISCUSSION

The electron-density distribution of the paraelectric tetragonal phase is first discussed. As clearly shown in Fig. 4,

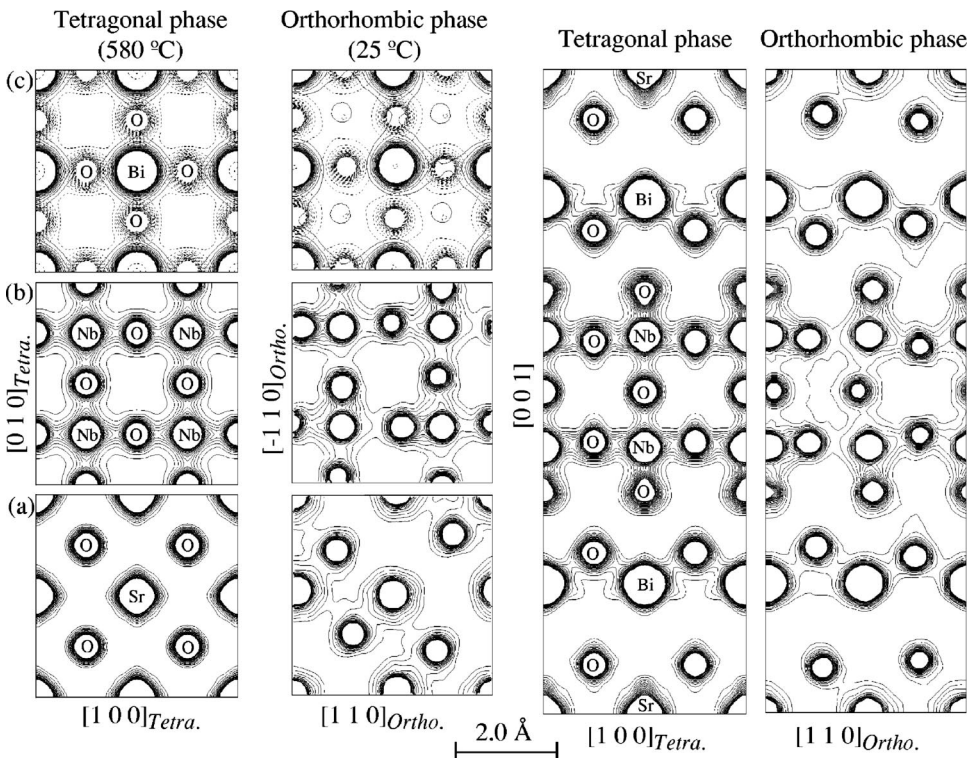


FIG. 4. Contour maps of electron-density distributions of paraelectric and ferroelectric  $\text{SrBi}_2\text{Nb}_2\text{O}_9$ . Maps (a)–(c) correspond to SrO, NbO<sub>2</sub>, and Bi<sub>2</sub>O<sub>2</sub> planes, respectively. In map (c), contours at positions of Bi and oxygen atoms in the Bi<sub>2</sub>O<sub>2</sub> layer are drawn with solid and dashed lines, respectively. Contour lines are drawn from 0.4 to 4.0  $e/\text{\AA}^3$  with 0.2  $e/\text{\AA}^3$  intervals. Note that  $a_{\text{Ortho}} \approx b_{\text{Ortho}} = \sqrt{2}a_{\text{Tetra}}$ .



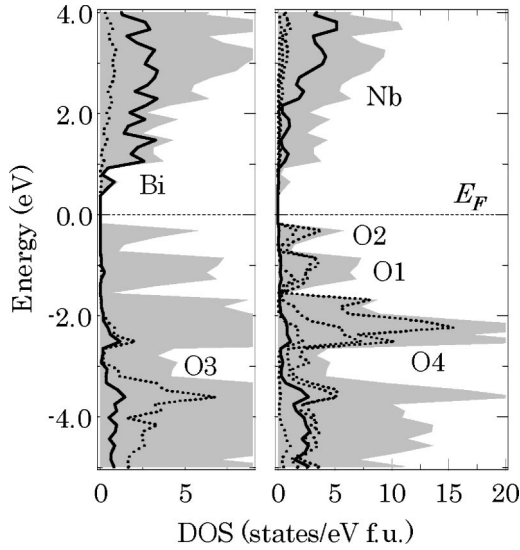


FIG. 5. Calculated total electronic density of states of  $\text{SrBi}_2\text{Nb}_2\text{O}_9$  (filled gray region). Partial density of states of Bi, Nb, and O are superimposed on the figure.  $E_F$  denotes the Fermi level.

bonding electrons around Nb atoms are found. These bonds originated from strong hybridization of orbitals between Nb and O atoms, as shown in the partial DOS in Fig. 5. The Nb(4d) orbital, which is empty in a simple ionic model, strongly hybridizes with the O(2p) orbital below the Fermi level ( $E_F$ ), and this hybridization makes the bonds covalent, forming a  $\text{NbO}_6$  octahedron. Minimum electron densities are  $1.33 \text{ e}/\text{\AA}^3$  for the bondings between Nb and O atoms in the  $\text{NbO}_2$  plane, and  $0.90$  and  $2.04 \text{ e}/\text{\AA}^3$  for those to the apex oxygen (Table II). Because of the short distance between Nb and O2 atoms (about  $1.76 \text{ \AA}$  from the preliminary Rietveld refinement), the electron density of the bond is large.

Bonding electrons between Bi and O3 atoms in the  $\text{Bi}_2\text{O}_2$  layer were also identified. Since the Bi atom has expanded lone-pair 6s electron orbitals, hybridization of Bi(6s) with O(2p) occurs despite a relatively long Bi-O bond length of about  $2.34 \text{ \AA}$ . This hybridization of orbitals is confirmed by the mixed partial DOS of Bi and O3. That is, the Bi(6s) partial density of states well hybridizes with O(2p) in the  $\text{Bi}_2\text{O}_2$  layer below  $-2 \text{ eV}$ . The surroundings of the Sr ion, on the other hand, have almost no bonding electron, indicating a pure ionic state of Sr. The estimated minimum electron density of about  $0.19 \text{ e}/\text{\AA}^3$  is comparable to the experimental background level.

The transition from a paraelectric tetragonal to ferroelec-

TABLE II. Minimum electron density ( $\text{e}/\text{\AA}^3$ ) of each bonding estimated from the electron-density distribution by MEM.

	Tetragonal phase	Orthorhombic phase
Sr-O1	$0.19 (\times 4)$	0.17, 0.21, 0.42, 0.65
Nb-O1	0.90	0.63
Nb-O2	2.04	1.40
Nb-O4	$1.33 (\times 4)$	0.51, 0.93, 1.20, 1.95
Bi-O3	$0.81 (\times 4)$	0.54, 0.67, 0.71, 0.71

tric orthorhombic phase induces large distortions in the crystal structure. Such distortions are evidently “visualized” in the electron-density distributions shown in Fig. 4. The most significant change in the distributions is seen in the bondings in the  $\text{NbO}_6$  octahedron: Four equivalent Nb-O4 bonds in the  $\text{NbO}_2$  plane of the tetragonal phase became inequivalent, and one of the bonds had a strong covalent character indicated by the increase of electron density from  $1.33$  to  $1.95 \text{ e}/\text{\AA}^3$ . In contrast, the electron density of another Nb-O4 bond decreased to  $0.51 \text{ e}/\text{\AA}^3$ . This low density implies that one of the covalent bonds in the orthorhombic structure almost “broke.” The minimum electron densities between Nb and apex oxygen atoms (O1 and O2) also decreased, suggesting weakened bonds. This anisotropic electron-density distribution is a result of enhanced orbital hybridization between the Nb(4d) and O(2p) orbitals below the ferroelectric Curie temperature. Strong covalent interaction on one of the bonds in the  $\text{NbO}_2$  plane causes the ferroelectric structural distortions, leading to displacive ferroelectric polarization. These changes in electron-density distribution are quite similar to those observed in ferroelectric PTO and BTO.<sup>14–17</sup> In PTO and BTO, the strong orbital hybridization of the Ti(3d) and O(2p) orbitals produced very short covalent bonds in the  $\text{TiO}_6$  octahedron and led to the ferroelectric instability.

The changes in the surroundings of the Sr ion were also found. In the orthorhombic ferroelectric phase, weak hybridization of electrons of Sr and O atoms are clearly seen in the electron-density distribution. The estimated electron density in the region between Sr and O1 atoms increased from  $0.19$  to  $0.65 \text{ e}/\text{\AA}^3$ . Although the main energy level of the Sr(5s) orbital is much higher than  $E_F$ , weak hybridization between the Sr(5s) and O(2p) orbitals appears to play an important role in the structural distortion and the ferroelectric polarization. This finding is also similar to that regarding covalency in the Pb-O bond in ferroelectric PTO.<sup>14–17</sup> The hybridization of the Pb(6s) with O(2p) orbitals apparently enhances the ferroelectric distortions.

Interestingly, the minimum electron densities of Bi-O3 bonds in the  $\text{Bi}_2\text{O}_2$  layer were not changed much by the phase transition at  $T_C$ , despite the distortion of the structure. Although weak bonding due to the hybridization of the Bi(6s,6p) and O(2p) orbitals exists in the  $\text{Bi}_2\text{O}_2$  layer of both paraelectric tetragonal and ferroelectric orthorhombic phases, these bonds appear to play a minor role in the ferroelectricity in  $\text{SrBi}_2\text{Nb}_2\text{O}_9$ . The Bi(6p) orbital, however, appears to be responsible for the electric response of the material. As shown by the DOS in Fig. 5, the bottom of the conduction band mainly consists of the Bi(6p) orbital. Thus, the electric characteristics, such as leakage current behavior, could be described as the nature of the Bi(6p) orbital.

#### IV. SUMMARY

Crystal structures and electron densities of paraelectric and ferroelectric  $\text{SrBi}_2\text{Nb}_2\text{O}_9$  were analyzed. The paraelectric phase ( $580^\circ\text{C}$ ) had  $I4/mmm$  tetragonal symmetry, and the ferroelectric phase ( $25^\circ\text{C}$ ) had  $A2_1am$  orthorhombic symmetry with large structural distortions. Electron-density

distributions obtained by MEM from synchrotron x-ray-diffraction data well reproduced the atomic arrangements of the material, and bonding electrons were clearly seen in the Nb-O bond in the octahedron and in the Bi-O bond in the Bi<sub>2</sub>O<sub>2</sub> layer. These covalent bonds originated from orbital hybridization, as clearly shown in the mixed partial density of states in the electronic-structure calculations. Comparison of the electron-density distributions of the paraelectric and ferroelectric phases revealed that the hybridization between

the Nb(4*d*) and O(2*p*) orbitals was enhanced in the ferroelectric phase and that one of the Nb-O bonds in the NbO<sub>6</sub> octahedron had a strong covalent character below the ferroelectric Curie temperature. Weak hybridization of the Sr(5*s*) with O(2*p*) orbitals was also observed. The above-described results are similar to those observed in the case of ferroelectric PbTiO<sub>3</sub>, and they clearly demonstrate that covalency due to orbital hybridization plays an important role in the structural distortion and ferroelectric polarization.

- 
- <sup>1</sup>C. A-Paz de Araujo, J. D. Cuchiaro, L. D. McMillan, M. C. Scott, and J. F. Scott, *Nature (London)* **374**, 627 (1995).
- <sup>2</sup>K. Amanuma, T. Hase, and Y. Miyasaka, *Appl. Phys. Lett.* **66**, 221 (1995).
- <sup>3</sup>B. Aurivillius, *Ark. Kemi* **1**, 463 (1949).
- <sup>4</sup>B. Aurivillius, *Ark. Kemi* **1**, 499 (1949).
- <sup>5</sup>B. Aurivillius, *Ark. Kemi* **2**, 519 (1950).
- <sup>6</sup>E. C. Subbarao, *J. Phys. Chem. Solids* **23**, 665 (1962).
- <sup>7</sup>Y. Shimakawa, Y. Kubo, Y. Nakagawa, T. Kamiyama, H. Asano, and F. Izumi, *Appl. Phys. Lett.* **74**, 1904 (1999).
- <sup>8</sup>Y. Shimakawa, Y. Kubo, Y. Nakagawa, S. Goto, T. Kamiyama, H. Asano, and F. Izumi, *Phys. Rev. B* **61**, 6559 (2000).
- <sup>9</sup>Y. Shimakawa and Y. Kubo, in *Ferroelectric Thin Films VIII*, edited by R. W. Schwartz, P. C. McIntyre, Y. Miyasaka, S. R. Summerfelt, and D. Wouters, *Mater. Res. Soc. Symp. Proc. No. 596* (Materials Research Society, Pittsburgh, 2000), p. 131.
- <sup>10</sup>Y. Shimakawa, Y. Kubo, Y. Tauchi, T. Kamiyama, H. Asano, and F. Izumi, *Appl. Phys. Lett.* **77**, 2749 (2000).
- <sup>11</sup>Y. Shimakawa, Y. Kubo, Y. Tauchi, H. Asano, T. Kamiyama, F. Izumi, and Z. Hiroi, *Appl. Phys. Lett.* **79**, 2791 (2001).
- <sup>12</sup>Ismunandar, B. J. Kennedy, Gunawan, and Marsongkohadi, *J. Solid State Chem.* **126**, 135 (1996).
- <sup>13</sup>S. M. Blake, M. J. Falconer, M. McCreedy, and P. Lightfoot, *J. Mater. Chem.* **7**, 1609 (1997).
- <sup>14</sup>R. E. Cohen and H. Krakauer, *Phys. Rev. B* **42**, 6416 (1990).
- <sup>15</sup>R. E. Cohen, *Nature (London)* **358**, 136 (1992).
- <sup>16</sup>R. E. Cohen and H. Krakauer, *Ferroelectrics* **136**, 65 (1992).
- <sup>17</sup>Y. Kuroiwa, S. Aoyagi, A. Sawada, J. Harada, E. Nishibori, M. Takata, and M. Sakata, *Phys. Rev. Lett.* **87**, 217601 (2001).
- <sup>18</sup>M. Sakata and M. Sato, *Acta Crystallogr., Sect. A: Found. Crystallogr.* **A46**, 263 (1990).
- <sup>19</sup>M. Takata and M. Sakata, *Acta Crystallogr., Sect. A: Found. Crystallogr.* **A52**, 287 (1996).
- <sup>20</sup>C. H. Hervoches, J. T. S. Irvine, and P. Lightfoot, *Phys. Rev. B* **64**, 100102 (2001).
- <sup>21</sup>R. Macquart, B. J. Kennedy, B. A. Hunter, C. J. Howard, and Y. Shimakawa (unpublished).
- <sup>22</sup>S. Kumazawa, Y. Kubota, M. Takata, M. Sakata, and Y. Ishibashi, *J. Appl. Crystallogr.* **26**, 453 (1993).
- <sup>23</sup>R. Macquart, B. J. Kennedy, and Y. Shimakawa, *J. Solid State Chem.* **160**, 174 (2001).
- <sup>24</sup>V. R. Saunders, R. Dovesi, C. Roetti, M. Causa, N. M. Harrison, R. Orlando, and C. M. Zicovich-Wilson, *CRYSTAL98 User's Manual* (University of Torino, Torino, Italy, 1998).
- <sup>25</sup>See, <http://www.theochem.uni-stuttgart.de/>